

Impact of Transition Metal Cations on the ^{29}Si NMR Signal in Metal Oxide Glasses: A DFT Case Study of Hafnia Silica Glass

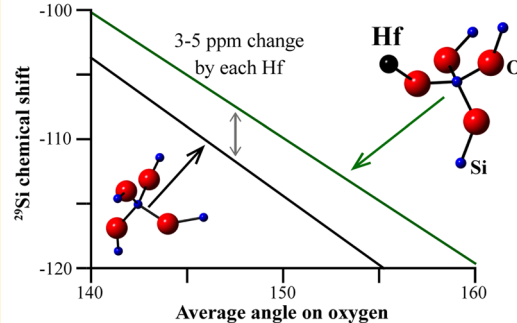
Ilia Ponomarev^{ID} and Peter Kroll^{*ID}

Department of Chemistry and Biochemistry, The University of Texas at Arlington, 700 Planetarium Place, Arlington, Texas 76019, United States

S Supporting Information

ABSTRACT: We investigate ^{29}Si nuclear magnetic resonance (NMR) chemical shifts δ_{iso} of soda-silica and hafnia-soda-silica glass models by structural modeling and the gauge-invariant projector augmented wave (GIPAW) method within density functional theory (DFT). Models of soda-silica glasses with molar ratios $\text{Na}_2\text{O}:\text{SiO}_2$ of 1:2 and 1:3 and hafnia content of 0–10 mol % are generated via a melt-quench procedure and ab initio molecular dynamic simulations. By correlating computed chemical shifts with structural data we establish angular correlation functions for Q^2 , Q^3 , and Q^4 units in soda-silica glasses. Addition of hafnia to soda-silica glasses results in 6-coordinated Hf surrounded by bridging O under avoidance of direct linkages between Hf-centered octahedra. Hf impacts the structural information that can be gathered from ^{29}Si NMR analysis profoundly: each Hf in second coordination to Si shifts the angular correlation function for $\text{Si}-\text{O}-\text{X}$ ($\text{X} = \text{Si}, \text{Hf}$) angles by 3–5 ppm. Hence, NMR signals of Q^2 and Q^3 units may overlap depending on the number of Hf surrounding Si. By substituting H for Na we convert the glass models into models of sol–gel derived $\text{HfO}_2-\text{SiO}_2$. The profound impact of Hf on the chemical shift of ^{29}Si calls for a reinterpretation of ^{29}Si NMR peaks observed for hafnia-silica glasses.

Correlating Bond Angles with ^{29}Si Chemical Shifts



1. INTRODUCTION

Hafnia (HfO_2) increases the chemical durability of silica-based glasses.^{1,2} Hafnia, like some other metal oxides, also increases hardness of glasses and glass-ceramic materials.^{3,4} Sol–gel derived hafnia-silica glasses and thin $\text{HfO}_2-\text{SiO}_2$ films find broad applications in optical and dielectric materials.^{5–8} Since hafnia is both a surrogate for PuO_2 and a good neutron absorber, it is also a benign component for the investigation of nuclear waste glasses.^{1,2,9}

Solid-state NMR provides insight into the local environments of atoms and is a powerful method to study materials.¹⁰ In particular, structural analysis of amorphous solids and glasses benefits from NMR studies, once the influence of the local environment on NMR parameters of a nucleus is established. With the advent of DFT calculations combined with the GIPAW method,¹¹ modeling and simulation have substantially augmented the information content of experimental NMR spectra of disordered systems. Solid-state NMR studies enhanced with DFT calculations have become an indispensable analytical tool to characterize short and medium range order in glasses.^{12–15}

In this study we explore the impact of Hf in hafnia-soda-silica glasses on ^{29}Si NMR chemical shift by combined DFT-GIPAW calculations.¹¹ First we investigate ^{29}Si NMR chemical shifts of crystalline silica polymorphs and sodium silicates. Then we investigate amorphous soda-silica and establish a correlation between $\text{Si}-\text{O}-\text{Si}$ angles and the chemical shift δ_{iso} .

of adjacent Si atoms. Subsequently, we add hafnia to the glass network and elucidate the impact of Hf as second-nearest neighbor to ^{29}Si on its chemical shift. Finally, replacing Na by H gives us access to models of hafnia-silica sol–gel materials, for which we provide new interpretations of their ^{29}Si NMR data.

2. METHODS

All our simulations are within density functional theory¹⁶ using the Vienna ab initio simulation (VASP) package.^{17,18} We use the projector augmented wave (PAW) method^{19,20} and approximate electron exchange and correlation by the Perdew–Burke–Ernzerhof (PBE) generalized gradient approximation (GGA). We sample the Brillouin zone at the Γ -point only for amorphous models, while we choose appropriate k -point meshes for crystalline models. For final optimizations of amorphous as well as crystalline models we rely on standard pseudopotentials provided with the VASP package and use an energy cutoff of 500 eV for the expansion of the wave function into the plane-wave basis set.

We generate models of soda-silica and hafnia-soda-silica glasses using a “melt-quench” approach together with Born–Oppenheimer ab initio molecular dynamics (aiMD) simulation.

Received: June 21, 2017

Revised: October 16, 2017

Published: October 16, 2017

Efficient model generation uses a “softer” version of the oxygen pseudopotential provided by VASP, a time-step $\Delta t = 2.0$ fs, and a cutoff of 283 eV at this stage. The temperature of the system is adjusted by velocity scaling. The temperature–time profile for our melt-quench scheme is shown in Figure 1.

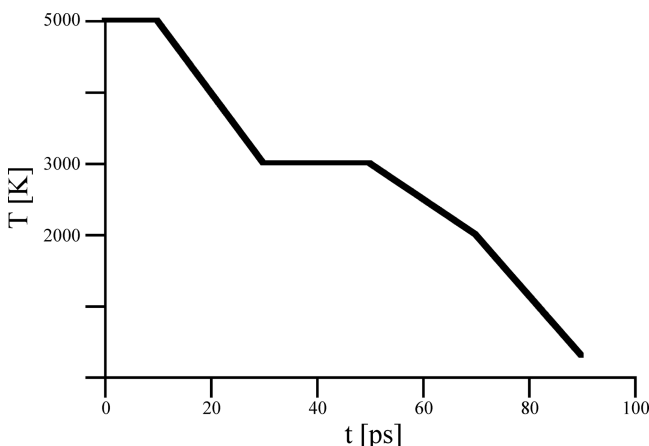


Figure 1. Temperature–time ($T-t$) profile for the melt-quench procedure to produce amorphous models. With a time-step $\Delta t = 2.0$ fs, the total time of 90 ps corresponds to 45 000 time steps.

Once the last configuration of the trajectory (at 300 K) is obtained, we switch back to the “standard” parameters and optimize the model allowing atomic positions and cell parameters to adjust to a local energy minimum state. For amorphous models, forces are converged to 5×10^{-2} eV/Å and stresses to lower than 2 kbar. In total we consider 40 models of soda-silica glasses consisting of 108 atoms and 246 models of hafnia-soda-silica glasses comprised of 108 to 120 atoms.

The NMR calculations are carried out using the GIPAW algorithm¹¹ as implemented in the VASP code. We choose an energy cutoff of 600 eV and find ^{29}Si NMR chemical shifts converged to better than 0.2 ppm.

For reference calculations, we select the following crystal structures from the Inorganic Crystal Structure Database: SiO_2 α -quartz,²¹ SiO_2 α -cristobalite,²² SiO_2 coesite,²³ Na_2SiO_3 ,²⁴ $\alpha\text{-Na}_2\text{Si}_2\text{O}_5$,²⁵ $\beta\text{-Na}_2\text{Si}_2\text{O}_5$,²⁶ and $\text{C-Na}_2\text{Si}_2\text{O}_5$.²⁷ For these structures we optimize atomic positions under the constraint of experimental lattice parameter. Forces are optimized to lower than to 5 meV/Å. Computed values of absolute chemical shifts are given in Table 1 and shown Figure 2.

Several approaches have been proposed to calibrate the computed absolute shifts σ_{iso} to correlate to experimental data.^{28,29} Here we choose a simple gauge by fitting a line with slope of 1 to the data of Table 1, see Figure 1. We obtain

$$\delta_{\text{iso}} = \sigma_{\text{iso}} + 330.9 \quad (1)$$

, and almost all values of δ_{iso} obtained this way are within 1 ppm of experimental data. Stronger deviations are observed only for α -cristobalite, coesite, and $\alpha\text{-Na}_2\text{Si}_2\text{O}_5$.

3. RESULTS AND DISCUSSION

3.1. ^{29}Si NMR of Soda-Silica Glasses. We modeled soda-silica glasses of two different compositions, with ratios $\text{Na}_2\text{O}/\text{SiO}_2$ of 1:2 and 1:3. These compositions are conventionally abbreviated as NS33 and NS25, respectively,

Table 1. Experimental ^{29}Si NMR Chemical Shifts δ_{iso} , Computed Absolute Shifts σ_{iso} , and Predicted δ_{iso} for Silica and Sodium Silicate Polymorphs^a

structure	δ_{iso} exp [ppm]	σ_{iso} comp [ppm]	δ_{iso} pred [ppm]
α -quartz	-107.1 ²⁸	-437.2	-106.4
α -cristobalite	-108.5 ²⁸	-437.8	-107.0
coesite Si[1]	-113.9 ²⁸	-446.8	-116.0
coesite Si[2]	-108.1 ²⁸	-439.3	-108.5
Na_2SiO_3	-76.8 ²⁸	-406.9	-76.1
$\alpha\text{-Na}_2\text{Si}_2\text{O}_5$	-94.2 ²⁸	-426.7	-95.9
$\beta\text{-Na}_2\text{Si}_2\text{O}_5$ Si[1]	-86.3 ²⁸	-417.2	-86.4
$\beta\text{-Na}_2\text{Si}_2\text{O}_5$ Si[2]	-88.2 ²⁸	-418.3	-87.5
$\text{C-Na}_2\text{Si}_2\text{O}_5$ Si[1]	-87.4 ²⁷	-418.0	-87.2
$\text{C-Na}_2\text{Si}_2\text{O}_5$ Si[2]	-86.3 ²⁷	-417.2	-86.4
$\text{C-Na}_2\text{Si}_2\text{O}_5$ Si[3]	-86.0 ²⁷	-417.1	-86.3
$\text{C-Na}_2\text{Si}_2\text{O}_5$ Si[4]	-88.2 ²⁷	-418.7	-87.9

^aThe prediction is based on a fit to the data, see Figure 1 and eq 1.

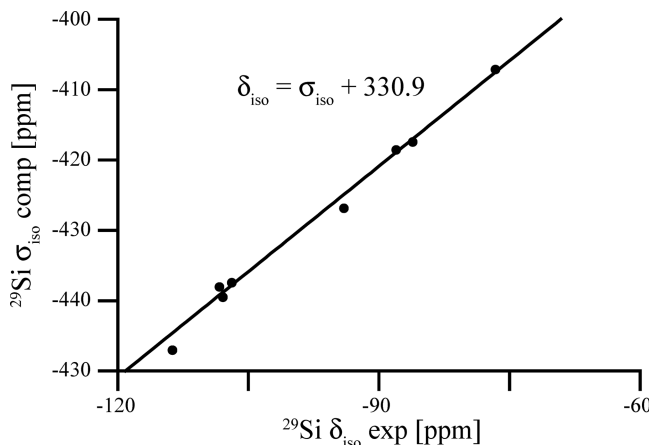


Figure 2. Correlation between experimental ^{29}Si NMR chemical shifts δ_{iso} and computed absolute shifts σ_{iso} for silica and sodium silicate polymorphs.

according to the mol-content Na_2O in the glass. We generated 13 models of NS25, $(\text{Na}_2\text{O})_9(\text{SiO}_2)_{27}$, and 27 models of NS33, $(\text{Na}_2\text{O})_{12}(\text{SiO}_2)_{24}$, each model comprising 108 atoms.

While the crystal structure of $\text{Na}_2\text{Si}_2\text{O}_5$ exhibits only Q^3 units, the NS33 glass models contain approximately 20% each of Q^4 and Q^2 units. This is somewhat higher than a fraction of 6% to 12.5% estimated from experimental observations.^{30,31} In our models we even observe a few Q^1 units. NS25 glass structures contain approximately 3% of Q^2 units and no Q^1 units. The average coordination number of Si is 4.1 for both NS25 and NS33 glasses, without any 3-fold coordinated Si, however. The average Si–O bond length in glass models is 1.65 Å, which is slightly longer than that found in amorphous silica models (1.62–1.63 Å)²⁹ and close to distances between Si and bridging O in silicates (e.g., 1.64 Å in $\alpha\text{-Na}_2\text{Si}_2\text{O}_5$ ²⁵ and $\beta\text{-Na}_2\text{Si}_2\text{O}_5$ ²⁶). The average Si–O–Si angle found in NS25 and NS33 models is 135°, which is approximately 10° smaller than inferred from experimental NMR data of soda-silica glasses.³²

Multiple studies, both experimental and computational, have shown that in silica structures the ^{29}Si NMR chemical shift δ_{iso} of tetrahedrally coordinated Si depend on the Si–O–Si bond angle Θ found at each neighboring oxygen atom.^{12,28,29,32–35} Different

functional dependencies on Θ have been formulated, such as $\sec(\Theta)$,³³ cosine expansions,¹² or a simple linear dependency.³⁴ Common to each approach is the assumption that contributions of each Si–O–Si bond angle surrounding the central Si are independent from each other. Charpentier et al. analyzed this in detail for amorphous silica.³⁵ Hence, the expression for the relation between δ_{iso} and Si–O–Si bond angle Θ is given by

$$\delta_{\text{iso}} = \frac{1}{n_{\text{BO}}} \sum_{i=1}^{n_{\text{BO}}} F(\Theta_{\text{Si}-\text{O}-\text{Si}}^i) \quad (2)$$

with $F(\Theta)$ being the explicit analytical form of the angular dependency. For Q^4 units, which are found in many silicate structures including amorphous silica, the number of non-bridging oxygens n_{BO} equals 4. The expression (2) above can be generalized for Q^3 [$n_{\text{BO}} = 3$] and Q^2 [$n_{\text{BO}} = 2$] units as well. We find that a simple linear function is sufficient to describe the angular dependency between δ_{iso} and Θ . This simplifies eq 2 to

$$\delta_{\text{iso}} = a_n + b_n \bar{\Theta}_{\text{Si}-\text{O}-\text{Si}} \quad (3)$$

Herein, $\bar{\Theta}_{\text{Si}-\text{O}-\text{Si}}$ is the average Si–O–Si angle found on adjacent O atoms, and a_n and b_n are coefficients to be determined for each Q^n unit. The same expression was previously used by Ispas et al. to describe chemical shifts of Q^4 , Q^3 , and Q^2 units in soda-silica and lithia-silica glasses.³² We have previously taken a similar approach to quantify ^{29}Si NMR chemical shifts in amorphous silica (SiO_2) and mixed $\text{SiO}_n\text{C}_{4-n}$ –tetrahedra in amorphous silicon oxycarbide (SiCO).²⁹

In Figure 3 we show the computed chemical shifts δ_{iso} for Q^n units ($n = 2–4$) from our collection of melt-quench modeled

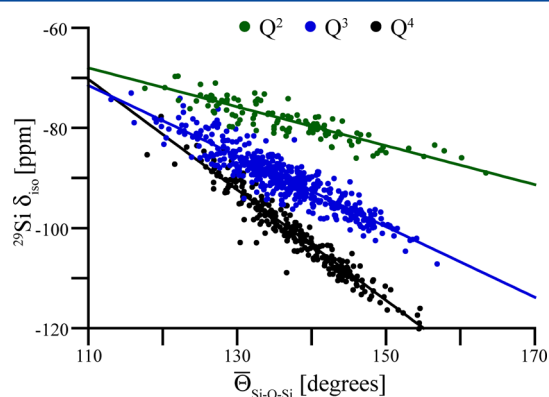


Figure 3. Computed ^{29}Si NMR chemical shift plotted versus average Si–O–Si angle on neighboring oxygens for Q^n vertices ($n = 2–4$) in soda-silica glasses (compositions $\text{Na}_2\text{O}:\text{SiO}_2$ of 1:2 and 1:3 are collected together). In total the graph contains data for more than 900 Si sites. The straight line is a linear fit to the data for each Q^n vertex.

soda-silica glass models (a total of more than 900 sites have been collected).

Linear fits to the data shown in Figure 1 provide the following angular correlation functions:

$$\begin{aligned} \delta_{\text{iso}}^{Q^4} &= (51.2 \pm 2.8) - (1.10 \pm 0.02) \bar{\Theta}_{\text{Si}-\text{O}-\text{Si}} \\ \delta_{\text{iso}}^{Q^3} &= (6.1 \pm 2.0) - (0.71 \pm 0.01) \bar{\Theta}_{\text{Si}-\text{O}-\text{Si}} \\ \delta_{\text{iso}}^{Q^2} &= (-25.2 \pm 2.5) - (0.39 \pm 0.02) \bar{\Theta}_{\text{Si}-\text{O}-\text{Si}} \end{aligned} \quad (4)$$

For each correlation we included the error from a least-squares fit into the expression. Ispas et al.³² determined fit coefficients $a_4 = 48.5$ and $b_4 = 1.07$ (Q^4 units) and $a_3 = 6.5$ and $b_3 = 0.70$ (Q^3 units). Hence, within the margin of error our results agree nicely with their data. For Q^2 units they obtained $a_2 = -44.6$ and 0.25, but their fit was based on only seven such Q^2 units. Our results, on the other side, analyze more than 100 Q^2 , 600 Q^3 , and 200 Q^4 units. Inspecting the residuals of our fits (see the Supporting Information), we find a Gaussian-like distribution with a fwhm of 5 ppm. The angular correlations collected in eq 4 also predict chemical shifts of crystalline sodium silicates (see Table 1) with a maximum deviation of 2 ppm between prediction on one side and experimental or directly computed values on the other side.

3.2. Impact of Hafnium on ^{29}Si NMR in Hafnia-Soda-Silica Glasses. Modeling of ternary hafnia-soda-silica glasses is achieved using the same melt-quench process as for the binary glasses. For both soda-silica glass compositions (NS33 and NS25), we added up to four units of HfO_2 to the model before starting the simulations. Hence, we generate models with compositions $(\text{HfO}_2)_k(\text{Na}_2\text{O})_{12}(\text{SiO}_2)_{24}$ and $(\text{HfO}_2)_k(\text{Na}_2\text{O})_9(\text{SiO}_2)_{27}$, with $k = 1–4$. The highest hafnia content corresponds to 10 mol % HfO_2 in the glass. This value relates to the solubility of 11 mol % hafnia in soda-silica glass with ~ 33 mol % of soda.⁹ We generated additional models starting from NS33 glass and changing Si atoms into Hf, formally morphing silica into hafnia. This yielded a series of compositions $(\text{HfO}_2)_k(\text{Na}_2\text{O})_{12}(\text{SiO}_2)_{24-k}$ ($k = 2, 4, 6, 8$, and 12).

We find that models with lowest energy after optimization exhibit octahedral $\text{HfO}_{6/2}^{2-}$ polyhedra with all six O atoms surrounding Hf bridging to the next Si. Hence, there is a strong avoidance to coordinate nonbridging O to Hf. We occasionally observe corner sharing of $\text{HfO}_{6/2}^{2-}$ –octahedra but never in energetically most favorable models and, overall, in amounts less than expected in a random mixing model. This is quite different from our results on hafnia-silica glasses (without soda), where hafnia units were found to cluster in low-energy models.³⁶ The difference highlights the impact of soda on the structure of these mixed metal oxide silica glasses. In ternary hafnia-soda-silica glasses $\text{HfO}_{6/2}^{2-}$ polyhedra form complex $\text{Hf}(\text{OSiO}_3)_6$ clusters, which are further embedded in the network either by bridging or nonbridging O at the outside of the cluster. Due to the definite coordination number and the well-defined local environment we regard Hf as network-forming element in these glasses. Nonbridging O atoms prefer bonding to Si, while Si itself is found in a variety of $Q^m_{m\text{Hf}}$ units, with different numbers m ($m = 0$ to n) of Hf in second coordination. However, since the basic $\text{HfO}_{6/2}^{2-}$ unit itself is charged (-2) , some of the bridging O coordinating to Hf have an associated Na cation close-by. This typical environment is illustrated in Figure 4.

Characterizing the ^{29}Si chemical shifts and their dependency on the local environment, we first focus on those Q^n units that exhibit only Si atoms as second-nearest neighbor. With no Hf in second-coordination, these units are labeled $Q^n_{0\text{Hf}}$. The relation between ^{29}Si NMR chemical shifts and the average angle of surrounding Si–O–Si angles is shown in Figure 5.

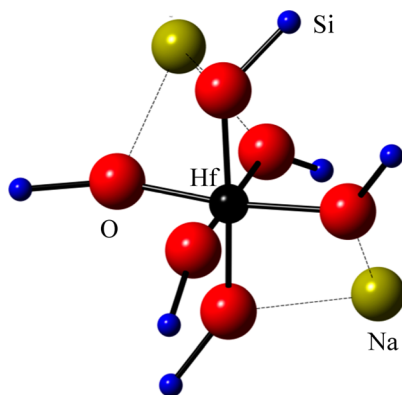


Figure 4. Characteristic chemical environment of Hf within a $[\text{HfO}_{6/2}]^{2-} \cdot 2\text{Na}^+$ unit in hafnia-soda-silica models.

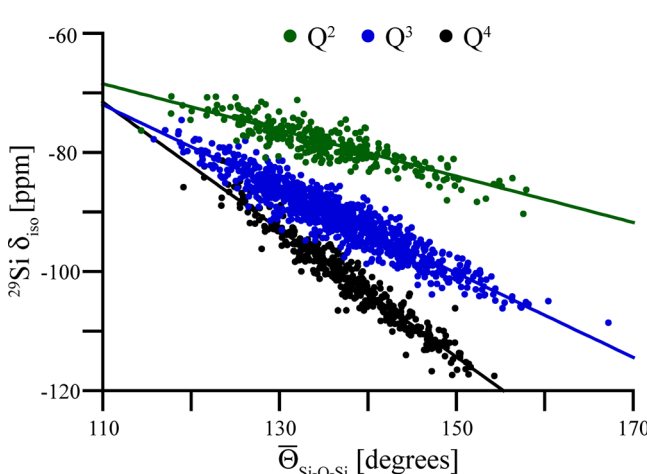


Figure 5. Relation between computed ^{29}Si NMR chemical shifts and average Si–O–Si angle on neighboring oxygens for Q_{Hf}^n vertices in hafnia-soda-silica glasses.

Once again we obtain linear angular correlation functions through a least-squares fit to the data:

$$\begin{aligned}\delta_{\text{iso}}^{\text{Q}^4} &= (46.1 \pm 1.9) - (1.07 \pm 0.01)\bar{\Theta}_{\text{Si}-\text{O}-\text{Si}} \\ \delta_{\text{iso}}^{\text{Q}^3} &= (5.7 \pm 1.2) - (0.71 \pm 0.01)\bar{\Theta}_{\text{Si}-\text{O}-\text{Si}} \\ \delta_{\text{iso}}^{\text{Q}^2} &= (-25.7 \pm 1.7) - (0.39 \pm 0.01)\bar{\Theta}_{\text{Si}-\text{O}-\text{Si}}\end{aligned}\quad (5)$$

For the range of angles that appear in our models, $115 < \Theta < 165$, the relations of eq 5 are consistent with those of eq 4, which were determined from soda-silica models free of hafnia. These results show that the chemical shift of Si within a $\text{Si}(\text{OSiO}_3)_4$ cluster, hence, Si with only Si atoms as next-nearest neighbors, is not impacted by adding hafnia to the glass. This changes, however, once Hf enters the coordination sphere of Si.

To analyze the chemical shifts of Q_{Hf}^m units, in which the central Si is surrounded by m Hf atoms as second-nearest neighbors, we assume that Si–O–Si and Si–O–Hf angles enter independently into the linear angular correlation function. This allows us to formulate the angular correlation function as a sum of two linear terms:

$$\begin{aligned}\delta_{\text{iso}} = \frac{1}{n_{\text{BO}}} \{ & \sum_{i=1}^{n_{\text{Si}}} (a_{n_{\text{BO}}}^{\text{Si}} + b_{n_{\text{BO}}}^{\text{Si}} \Theta_{\text{Si}-\text{O}-\text{Si}}^i) \\ & + \sum_{j=1}^{n_{\text{Hf}}} (a_{n_{\text{BO}}}^{\text{Hf}} + b_{n_{\text{BO}}}^{\text{Hf}} \Theta_{\text{Si}-\text{O}-\text{Hf}}^j) \}\end{aligned}\quad (6)$$

Parameters a^{Si} , b^{Si} , a^{Hf} , and b^{Hf} can be determined from the data for every Q^n unit, and results for Q_{Hf}^4 , Q_{Hf}^3 , and Q_{Hf}^2 units are shown in Figure 6.

We obtain as before linear angular correlation functions for Si–O–Si and Si–O–Hf angles in Q_{Hf}^4 , Q_{Hf}^3 , and Q_{Hf}^2 units:

$$\begin{aligned}\delta_{\text{iso}}^{\text{Q}^4} &= \frac{1}{4} \{ \sum_{i=1}^{n_{\text{Si}}} [(46.1 \pm 1.9) - (1.07 \pm 0.01)\Theta_{\text{Si}-\text{O}-\text{Si}}^i] \\ & + \sum_{j=1}^{n_{\text{Hf}}} [(5.6 \pm 4.0) - (0.68 \pm 0.02)\Theta_{\text{Si}-\text{O}-\text{Hf}}^j] \} \\ \delta_{\text{iso}}^{\text{Q}^3} &= \frac{1}{3} \{ \sum_{i=1}^{n_{\text{Si}}} [(5.7 \pm 1.2) - (0.71 \pm 0.01)\Theta_{\text{Si}-\text{O}-\text{Si}}^i] \\ & + \sum_{j=1}^{n_{\text{Hf}}} [(-23 \pm 12) - (0.39 \pm 0.01)\Theta_{\text{Si}-\text{O}-\text{Hf}}^j] \} \\ \delta_{\text{iso}}^{\text{Q}^2} &= \frac{1}{2} \{ \sum_{i=1}^{n_{\text{Si}}} [(-25.7 \pm 1.7) - (0.39 \pm 0.01)\Theta_{\text{Si}-\text{O}-\text{Si}}^i] \\ & + \sum_{j=1}^{n_{\text{Hf}}} [(-51 \pm 7) - (0.15 \pm 0.05)\Theta_{\text{Si}-\text{O}-\text{Hf}}^j] \}\end{aligned}\quad (7)$$

It turns out that the impact of Hf as second-nearest neighbor to Si is profound: comparing two Q^4 units with identical average bond angle $\bar{\Theta}$ but different numbers of Hf in second coordination, we find that each Hf changes the ^{29}Si chemical shift by 2.5 ppm ($\bar{\Theta} = 130^\circ$) to 5.5 ppm ($\bar{\Theta} = 160^\circ$).

This impact of Hf on the ^{29}Si NMR is quite significant in case we use NMR data to estimate the degree of condensation of the hafnia-silica network in hafnia-soda-silica glasses or, for example, in sol–gel derived hafnia-silica products. The point is that Q_{Hf}^n units may easily be misinterpreted as $\text{Q}_{\text{Hf}}^{n-1}$ units with the consequence that the connectivity of the network will be severely mischaracterized. This is best illustrated for sol–gel derived glasses containing hafnia, which we will consider in the next section.

3.3. Substitution of Sodium into Hydrogen. Sol–Gel Hafnia–Silica Glasses. Hafnia-silica materials find a wide range of applications in optics and dielectric materials. For example, hafnon (HfSiO_4) is a potential high- κ dielectric material,³⁷ and hafnia-silica thin films are used as high refractive index coatings in LIGO, the Laser Interferometric Gravitational Wave Observatory.³⁸ Due to the low solubility of hafnia in silica (only up to 4 mol %³⁹), the sol–gel route is commonly used to obtain hafnia-silica glasses with high hafnia content. ^{29}Si NMR is then routinely used to characterize the degree of condensation (or amount of “disruption”) of the network built during the gelation process.⁷ Evidently, understanding the impact of Hf on ^{29}Si NMR chemical shifts in this type of materials is critical.

Our hafnia-soda-silica glass models are simply converted into models for sol–gel derived hafnia-silica by changing sodium atoms (Na) into hydrogen (H). Since Na and H

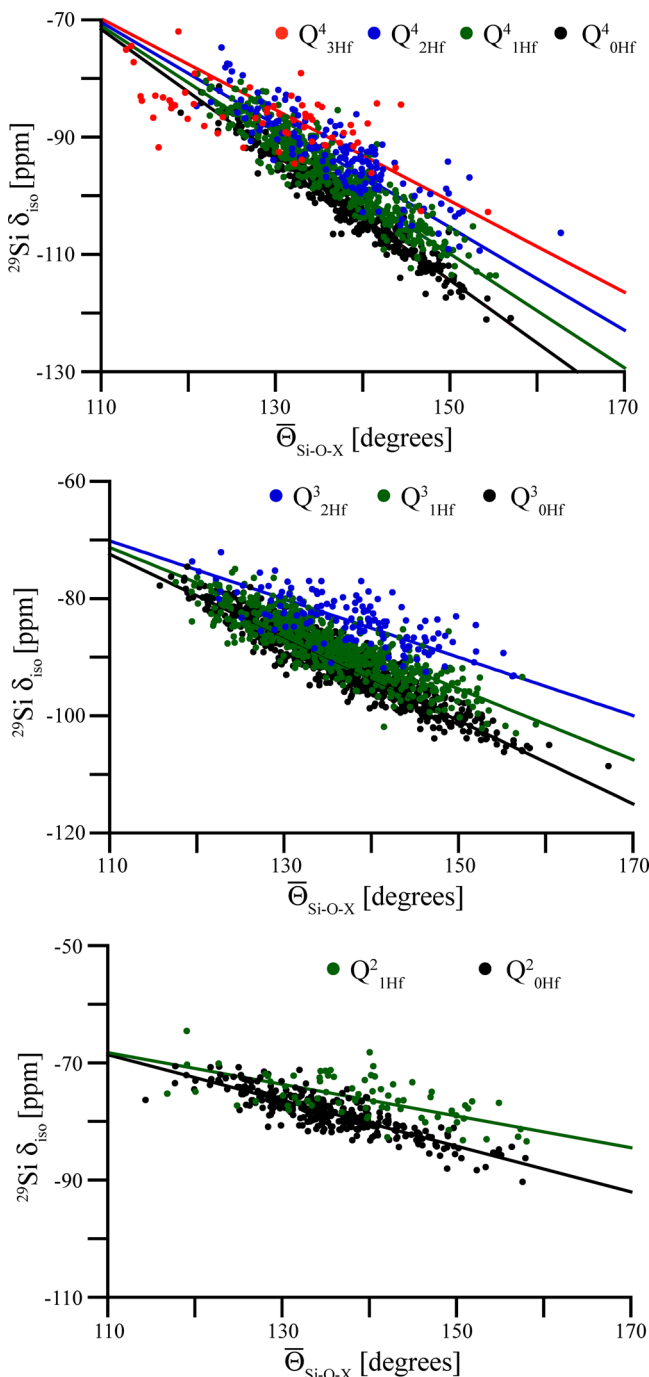


Figure 6. Relation between average Si–O–X angle (X = Si, Hf) and ^{29}Si NMR chemical shift for $Q^4_{n\text{Hf}}$ (top), $Q^3_{n\text{Hf}}$ (center), and $Q^2_{n\text{Hf}}$ (bottom) units in hafnia-soda-silica glasses.

have different distances to adjacent O atoms, we optimize the H positions while keeping cell parameters and positions of all other elements, Hf, Si, and O, fixed. This procedure facilitates the study of the impact of protons (H^+), which bond covalently to a single O, in contrast to Na cations, which are “embedded” by surrounding O. Since the remaining Si–O–Hf network remains unchanged, all geometrical parameters (distances and angles) relevant for angle correlation functions are the same as before for soda-silica models. We once again compute the NMR data and show results for Q^4 and Q^3 vertices in Figure 7.

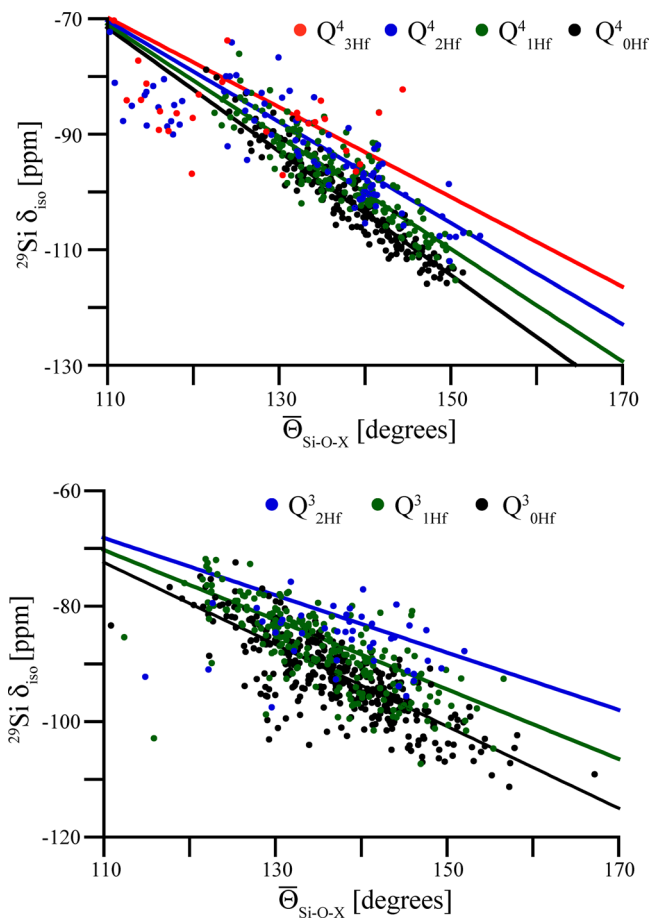


Figure 7. Relation between average Si–O–X angle and ^{29}Si NMR chemical shift for $Q^4_{n\text{Hf}}$ (left) and $Q^3_{n\text{Hf}}$ (right) vertices in hafnia-silica sol–gel glasses. Fit residuals for Q^4 units are given in the Supporting Information.

The data is once again used to fit a model similar to that presented in eq 6 but this time for $\text{HfO}_2\text{–H}_2\text{O–SiO}_2$ models. The resulting parameters are given in eq 8:

$$\begin{aligned} \delta_{\text{iso}}^{Q^4} &= \frac{1}{4} \left\{ \sum_{i=1}^{n_{\text{Si}}} [(54 \pm 4) - (1.12 \pm 0.03) \Theta_{\text{Si–O–Si}}^i] \right. \\ &\quad \left. + \sum_{j=1}^{n_{\text{Hf}}} [(4.0 \pm 6.0) - (0.59 \pm 0.04) \Theta_{\text{Si–O–Hf}}^j] \right\} \\ \delta_{\text{iso}}^{Q^3} &= \frac{1}{3} \left\{ \sum_{i=1}^{n_{\text{Si}}} [(6.0 \pm 3.8) - (0.71 \pm 0.03) \Theta_{\text{Si–O–Si}}^i] \right. \\ &\quad \left. + \sum_{j=1}^{n_{\text{Hf}}} [(-20 \pm 8) - (0.46 \pm 0.06) \Theta_{\text{Si–O–Hf}}^j] \right\} \\ \delta_{\text{iso}}^{Q^2} &= \frac{1}{2} \left\{ \sum_{i=1}^{n_{\text{Si}}} [(-25 \pm 16) - (0.42 \pm 0.12) \Theta_{\text{Si–O–Si}}^i] \right. \\ &\quad \left. + \sum_{j=1}^{n_{\text{Hf}}} [(-66 \pm 18) - (0.08 \pm 0.12) \Theta_{\text{Si–O–Hf}}^j] \right\} \end{aligned} \quad (8)$$

These parameters do not differ substantially from those for hafnia-soda-silica glasses given in eq 7. Consequently, the ^{29}Si chemical shift in sol–gel derived hafnia-silica glasses is profoundly impacted by the presence of Hf as second-nearest neighbor: for an average bond angle $\bar{\Theta}$ of 140° the change amounts to 4 ppm for each Hf.

To illustrate the impact, we analyze experimental data of O’Dell et al.⁷ The authors characterize the relative proportions of

Q^2 , Q^3 , and Q^4 units in an unheated sol–gel derived $(\text{HfO}_2)_{0.1}(\text{SiO}_2)_{0.9}$ glass by ^{29}Si NMR. The experimental spectrum is shown in Figure 8 (top) together with their fitting, which assumes three Gaussians centered at -93.7 , -101.2 , and -108.7 ppm for Q^2 , Q^3 , and Q^4 units, respectively. The relative

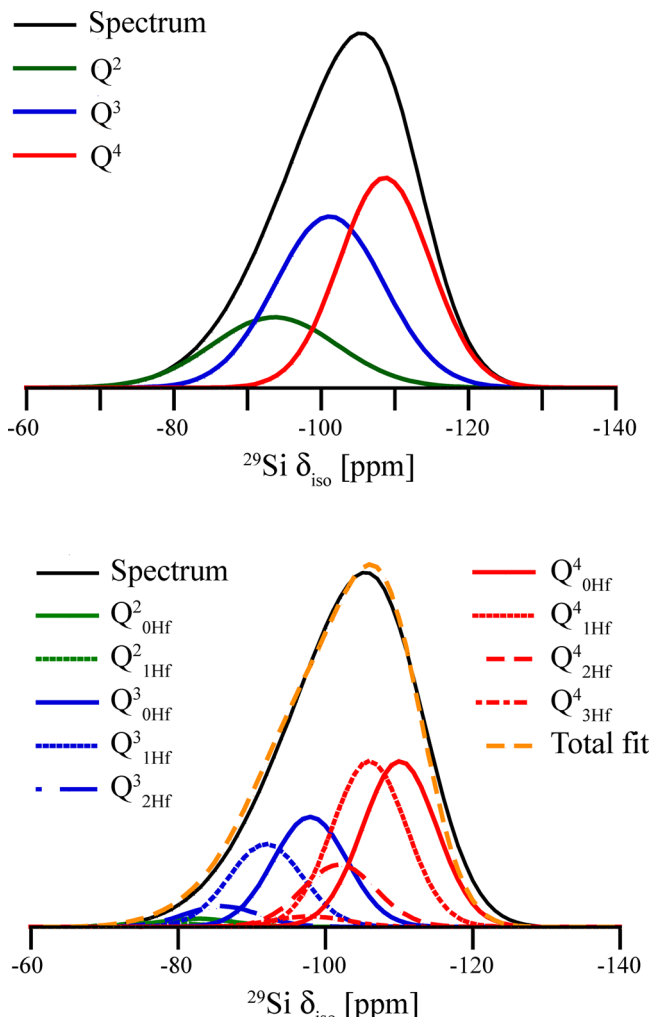


Figure 8. ^{29}Si NMR spectrum of unheated sol–gel derived $(\text{HfO}_2)_{0.1}(\text{SiO}_2)_{0.9}$ glass. Top: fitting of O'Dell et al.;⁷ bottom: analysis presented here.

intensities of peaks $Q^2:Q^3:Q^4$ are 19:40:41 and yield a fraction of NBO's of 33%.

However, we find that the peak assignment of O'Dell et al. is inconsistent with our results. A Q^4 peak located at -108.7 ppm indicates an average bond angle $\bar{\Theta}$ of 146° , a Q^3 peak located at -101.2 ppm suggests $\bar{\Theta}$ of 154° , and a Q^2 peak located at -93.7 ppm relates to $\bar{\Theta}$ of 179° . Although these predicted angles do not need to be identical (indeed, the various Q^n species may have different involvement in rings of different size), the angles at Q^2 units would be extreme. Typical Si–O–Si angles in silica glasses are around 145° , based on neutron scattering data.⁴⁰ Besides, the peak assignment of O'Dell et al. ignores the impact of Hf as second nearest neighbor to Si.

We, therefore, contrast the evaluation of O'Dell et al.⁷ by our own analysis (details provided in the Supporting Information), which is shown in Figure 8 on the bottom. We fit the same experimental data assuming random connectivity of silica and hafnia units and applying the angular correlation functions

for Q^n_{Hf} units of eq 8. We further assume equal average bond angles $\bar{\Theta}$ and equal width of the distribution for all Q^n units, independent of the number of Hf coordinating the Si. We extract from the data an average Si–O–X bond angle $\bar{\Theta}$ of 146° , which is consistent with typical Si–O–Si angles in silica glasses mentioned earlier. This outcome provides strong support for the relevance of our approach. The analysis, furthermore, yields relative amounts of $Q^2:Q^3:Q^4$ units of 2:34:64, which is strikingly different from the numbers extracted by O'Dell et al.⁷ Notably, the amount of Q^2 units is far lower than that proposed by O'Dell et al.⁷ As a consequence, we determine the fraction of NBO's to be 17%, less than half of the value stipulated by O'Dell et al.⁷ Ultimately, our analysis indicates a substantially higher degree of condensation in this material.

4. SUMMARY AND CONCLUSION

We studied ^{29}Si NMR chemical shifts in hafnia-soda-silica glass models using density functional theory calculations and GIPAW algorithm. Hf preferentially builds complex $[\text{HfO}_{6/2}]^{2-} \cdot 2\text{Na}^+$ units and is surrounded by bridging O only. The ^{29}Si NMR chemical shifts in Q^n units can be described well by linear angular correlation functions, treating the contributions of each surrounding Si–O–X angle independently. Hafnium impacts δ_{iso} of ^{29}Si once it appears as second-nearest neighbor to Si: for the same bond angle at O, the coordinating Hf changes the ^{29}Si chemical shift by 2.5–5.5 ppm for bond angles characteristic for such glass systems, 130 – 160° . We show that results obtained for hafnia-soda-silica glasses do transfer to sol–gel derived hafnia-silica glasses. Based on our results, we provide a new approach to analyze the condensation process of sol–gel glasses by ^{29}Si NMR. Applied to a sample system, our method yields average bond angles consistent with similar silica glasses but evinces substantially different proportions of various Q^n units. Consequently, our study demonstrates that proper analysis of ^{29}Si NMR data in sol–gel derived metal oxide glasses benefits from computational modeling and simulation.

ASSOCIATED CONTENT

Supporting Information

The Supporting Information is available free of charge on the ACS Publications website at DOI: 10.1021/acs.jpcc.7b06094.

Residuals of the fits mentioned and details of fitting the experimental NMR spectrum of sol–gel hafnia-silica glass. (PDF)

AUTHOR INFORMATION

Corresponding Author

*E-mail: pkroll@uta.edu.

ORCID

Ilia Ponomarev: 0000-0002-3321-6671

Peter Kroll: 0000-0003-4782-2805

Notes

The authors declare no competing financial interest.

ACKNOWLEDGMENTS

This work was supported by the NSF (CMMI-1634448 and DMR-1463974). Computational work was made possible through generous grants by the Texas Advance Computing Center in Austin, TACC, Texas.

■ REFERENCES

- Bergeron, B.; Galois, L.; Jollivet, P.; Angeli, F.; Charpentier, T.; Calas, G.; Gin, S. First Investigations of the Influence of IVb Elements (Ti, Zr, and Hf) on the Chemical Durability of Soda-Lime Borosilicate Glasses. *J. Non-Cryst. Solids* **2010**, *356*, 2315–2322.
- Hopf, J.; Kerisit, S. N.; Angeli, F.; Charpentier, T.; Icenhower, J. P.; McGrail, B. P.; Windisch, C. F.; Burton, S. D.; Pierce, E. M. Glass-Water Interaction: Effect of High-Valence Cations on Glass Structure and Chemical Durability. *Geochim. Cosmochim. Acta* **2016**, *181*, 54–71.
- Adams, R. W., Jr.; Clarke, D. R.; Knickerbocker, S. H.; Rapp, L. L.; Schwartz, B. Zirconia Toughening of Glass-Ceramic Materials. U.S. Patent 5,173,331, 1992.
- Adams, R. W., Jr.; Clarke, D. R.; Knickerbocker, S. H.; Rapp, L. L.; Schwartz, B. Zirconia Toughening of Glass-Ceramic Materials. U.S. Patent 5,185,215, 1993.
- Neumayer, D. A.; Cartier, E. Materials Characterization of ZrO_2 - SiO_2 and HfO_2 - SiO_2 Binary Oxides Deposited by Chemical Solution Deposition. *J. Appl. Phys.* **2001**, *90*, 1801–1808.
- Armelao, L.; Gross, S.; Muller, K.; Pace, G.; Tondello, E.; Tsetsgee, O.; Zattin, A. Structural Evolution Upon Thermal Heating of Nanostructured Inorganic-Organic Hybrid Materials to Binary Oxides MO_2 - SiO_2 ($M = Hf, Zr$) as Evaluated by Solid-State NMR and FTIR Spectroscopy. *Chem. Mater.* **2006**, *18*, 6019–6030.
- O'Dell, L. A.; Gunawidjaja, P. N.; Holland, M. A.; Mountjoy, G.; Pickup, D. M.; Newport, R. J.; Smith, M. E. Characterisation of Sol-Gel Prepared $(HfO_2)_{(X)}(SiO_2)_{(1-X)}$ ($X = 0.1, 0.2$ and 0.4) by H-1, C-13, O-17 and Si-29 MAS NMR, FTIR and TGA. *Solid State Nucl. Magn. Reson.* **2008**, *33*, 16–24.
- Kim, N.; Bassiri, R.; Fejer, M. M.; Stebbins, J. F. Structure of Amorphous Silica-Hafnia and Silica-Zirconia Thin-Film Materials: The Role of a Metastable Equilibrium State in Non-Glass-Forming Oxide Systems. *J. Non-Cryst. Solids* **2015**, *429*, 5–12.
- Davis, L. L.; Darab, J. G.; Qian, M.; Zhao, D.; Palenik, C. S.; Li, H.; Strachan, D. M.; Li, L. Hafnium in Peralkaline and Peraluminous Boro-Aluminosilicate Glass and Glass Sub-Components: A Solubility Study. *J. Non-Cryst. Solids* **2003**, *328*, 102–122.
- Charpentier, T.; Menziani, M. C.; Pedone, A. Computational Simulations of Solid State NMR Spectra: A New Era in Structure Determination of Oxide Glasses. *RSC Adv.* **2013**, *3*, 10550–10578.
- Pickard, C. J.; Mauri, F. All-Electron Magnetic Response with Pseudopotentials: NMR Chemical Shifts. *Phys. Rev. B: Condens. Matter Mater. Phys.* **2001**, *63*, 245101.
- Mauri, F.; Pasquarello, A.; Pfrommer, B. G.; Yoon, Y. G.; Louie, S. G. Si-O-Si Bond-Angle Distribution in Vitreous Silica from First-Principles Si-29 NMR Analysis. *Phys. Rev. B: Condens. Matter Mater. Phys.* **2000**, *62*, R4786–R4789.
- Ferlat, G.; Charpentier, T.; Seitsonen, A. P.; Takada, A.; Lazzeri, M.; Cormier, L.; Calas, G.; Mauri, F. Boroxol Rings in Liquid and Vitreous B_2O_3 from First Principles. *Phys. Rev. Lett.* **2008**, *101*, 065504.
- Pedone, A.; Charpentier, T.; Malavasi, G.; Menziani, M. C. New Insights into the Atomic Structure of 45SS Bioglass by Means of Solid-State NMR Spectroscopy and Accurate First-Principles Simulations. *Chem. Mater.* **2010**, *22*, 5644–5652.
- Gambuzzi, E.; Pedone, A.; Menziani, M. C.; Angeli, F.; Florian, P.; Charpentier, T. Calcium Environment in Silicate and Aluminosilicate Glasses Probed by Ca-43 MQMAS NMR Experiments and MD-Gipaw Calculations. *Solid State Nucl. Magn. Reson.* **2015**, *68*–69, 31–36.
- Hohenberg, P.; Kohn, W. Inhomogeneous Electron Gas. *Phys. Rev.* **1964**, *136*, B864.
- Kresse, G.; Hafner, J. Ab-Initio Molecular-Dynamics Simulation of the Liquid-Metal Amorphous-Semiconductor Transition in Germanium. *Phys. Rev. B: Condens. Matter Mater. Phys.* **1994**, *49*, 14251–14269.
- Kresse, G.; Furthmüller, J. Efficient Iterative Schemes for Ab Initio Total-Energy Calculations Using a Plane-Wave Basis Set. *Phys. Rev. B: Condens. Matter Mater. Phys.* **1996**, *54*, 11169–11186.
- Blochl, P. E. Projector Augmented-Wave Method. *Phys. Rev. B: Condens. Matter Mater. Phys.* **1994**, *50*, 17953–17979.
- Kresse, G.; Joubert, D. From Ultrasoft Pseudopotentials to the Projector Augmented-Wave Method. *Phys. Rev. B: Condens. Matter Mater. Phys.* **1999**, *59*, 1758–1775.
- Fujishita, H.; Hayashi, M.; Kanai, T.; Yamada, T.; Igawa, N.; Kihara, K. Study of Quantum Effects on Atomic Displacements in Quartz. *J. Phys. Chem. Solids* **2010**, *71*, 1285–1289.
- Dera, P.; Lazar, J. D.; Prakapenka, V. B.; Barkley, M.; Downs, R. T. New Insights into the High-Pressure Polymorphism of SiO_2 Cristobalite. *Phys. Chem. Miner.* **2011**, *38*, 517–529.
- Hill, R. J.; Gibbs, G. V.; Craig, J. R.; Ross, F. K.; Williams, J. M. Neutron-Diffraction Study of Hemimorphite. *Z. Kristallogr. - Cryst. Mater.* **1977**, *146*, 241–259.
- McDonald, W. S.; Cruickshank, D. W. A Refinement of Structure of S_3O . *Acta Crystallogr.* **1967**, *22*, 48.
- Pant, A. K.; Cruickshank, D. W. Crystal Structure of Alpha- $Na_2Si_2O_5$. *Acta Crystallogr., Sect. B: Struct. Crystallogr. Cryst. Chem.* **1968**, *24*, 13.
- Pant, A. K. A Reconsideration of Crystal Structure of Beta- $Na_2Si_2O_5$. *Acta Crystallogr., Sect. B: Struct. Crystallogr. Cryst. Chem.* **1968**, *24*, 1077.
- Rakic, S.; Kahlenberg, V.; Weidenthaler, C.; Zibrowius, B. Structural Characterization of High-Pressure C-Na(2)Si(2)O(5) by Single-Crystal Diffraction and (29)Si MAS NMR. *Phys. Chem. Miner.* **2002**, *29*, 477–484.
- Charpentier, T.; Ispas, S.; Profeta, M.; Mauri, F.; Pickard, C. J. First-Principles Calculation of O-17, Si-29, and Na-23 NMR Spectra of Sodium Silicate Crystals and Glasses. *J. Phys. Chem. B* **2004**, *108*, 4147–4161.
- Nimmo, J. P.; Kroll, P. First-Principles Calculations and Analysis of Si-29 Nuclear Magnetic Resonance Chemical Shifts in Silicon Oxycarbide Ceramics. *J. Phys. Chem. C* **2014**, *118*, 29952–29961.
- Mysen, B. O.; Frantz, J. D. Structure and Properties of Alkali Silicate Melts at Magmatic Temperatures. *Eur. J. Mineral.* **1993**, *5*, 393–407.
- Maekawa, H.; Maekawa, T.; Kawamura, K.; Yokokawa, T. The Structural Groups of Alkali Silicate-Glasses Determined from Si-29 MAS NMR. *J. Non-Cryst. Solids* **1991**, *127*, 53–64.
- Ispas, S.; Charpentier, T.; Mauri, F.; Neuville, D. R. Structural Properties of Lithium and Sodium Tetrasilicate Glasses: Molecular Dynamics Simulations Versus NMR Experimental and First-Principles Data. *Solid State Sci.* **2010**, *12*, 183–192.
- Smith, J. V.; Blackwell, C. S. Nuclear Magnetic-Resonance of Silica Polymorphs. *Nature* **1983**, *303*, 223–225.
- Oestrike, R.; Yang, W. H.; Kirkpatrick, R. J.; Hervig, R. L.; Navrotzky, A.; Montez, B. High-Resolution Na-23, Al-27, and Si-29 NMR-Spectroscopy of Framework Aluminosilicate Glasses. *Geochim. Cosmochim. Acta* **1987**, *51*, 2199–2209.
- Charpentier, T.; Kroll, P.; Mauri, F. First-Principles Nuclear Magnetic Resonance Structural Analysis of Vitreous Silica. *J. Phys. Chem. C* **2009**, *113*, 7917–7929.
- Dasmahapatra, A.; Kroll, P. Structure and Thermochemistry of Hafnium-Silicate Glasses. *Abstr. Pap. Am. Chem. Soc.* **2014**, 247.
- Monaghan, S.; Povey, I. Single Crystal High Dielectric Constant Material and Method for Making Same. U.S. Patent US20140332746 A1, 2014.
- Harry, G. M. Advanced Ligo: The Next Generation of Gravitational Wave Detectors. *Classical Quantum Gravity* **2010**, *27*, 084006.
- Ledneva, T. P.; et al. Solubility of the Refractory Oxides Zirconium Dioxide and Hafnium Dioxide in Silica. *Steklo* **1973**, *2*, 84–87.
- Grimley, D. I.; Wright, A. C.; Sinclair, R. N. Neutron-Scattering from Vitreous Silica IV. Time-of-Flight Diffraction. *J. Non-Cryst. Solids* **1990**, *119*, 49–64.